Correlating Quasi–Electron Relaxation with Quantum Femtosecond Magnetism in the Order Parameter Dynamics of Insulating Manganites

T. Li,[1] A. Patz,[1] P. Lingos,[2] L. Mouchliadis,[2] L. Li,[3] J. Yan,[3] I. E. Perakis,[2,4] and J. Wang[1]

[1] *Ames Laboratory and Department of Physics and Astronomy, Iowa State University, Ames, Iowa 50011, U.S.A.*

[2] *Department of Physics, University of Crete, Box 2208, Heraklion, Crete, 71003, Greece*

[3] *Department of Materials Science and Engineering, University of Tennessee, Knoxville, Tennessee 37996, U.S.A*

[4] *Institute of Electronic Structure & Laser, Foundation for Research and Technology–Hellas, Vassilika Vouton, 71110 Heraklion, Crete, Greece*

(Dated: September 8, 2014)

Femtosecond (fs)–resolved simultaneous measurements of charge and spin dynamics reveal the coexistence of two different quasi–particle excitations in colossal magneto-resistive (CMR) manganites, with *fs* and *ps* relaxation times respectively. Their populations reverse size above a *photoexcitation–intensity–threshold* coinciding with a "sudden" antiferro–to–ferromagnetic switching during <100 fs laser pulses. We present evidence that fast, metallic, mobile quasi–electrons dressed by *quantum spin fluctuations* coexist with slow, localized, polaronic charge carriers in non–equilibrium phases. This may be central to CMR transition and leads to a laser–driven charge reorganization simultaneously with quantum fs magnetism via an emergent quantum–spin/charge/lattice transient coupling.

PACS numbers: 78.67.Wj, 73.22.Pr, 78.47.J-,78.45.+h

arXiv:1409.1591v1 [cond-mat.str-el] 3 Sep 2014

Traditionally, quantum material phases are tuned by static parameters such as chemical dopants, pressure, or magnetic fields. *Spontaneous coherence* induced in this way, e.g. between many–body states separated by the Mott–Hubbard insulator gap, can establish new orders via equilibrium phase transitions. *Non–equilibrium* phase transitions may be similarly triggered by non–local, time–dependent electron–hole (e–h) coherence driven by a fs laser pulse [1, 2]. Due to the "sudden" time–dependent change in the Hamiltonian, the equilibrium state is no longer the ground state of the coupled light–matter system, which creates a quasi–instantaneous initial condition for time evolution of material phases. Strongly–correlated states, determined by many–electron ordering and coherence arising, e.g., when local interactions exceed or compare to the kinetic energy, are particularly responsive to such non–adiabatic excitations. In contrast, fs excitations merely perturb the *"rigid"* electronic bands of weakly–correlated materials (e.g. semiconductors). In the manganites, laser–driven bonding mediated by quantum spin flip/canting fluctuations was shown to induce a magnetic phase transition during <100fs pulses [3]. The *quantum femtosecond magnetism* originates from transient modification of inter–atomic e–hopping amplitude by the laser E–field [3], which *non–adiabatically* generates spin–exchange coupling and ferromagnetic correlation, as photoelectron hopping *simultaneously* flips local spins.

Complex materials such as manganites involve simultaneous ordering of multiple degrees of freedom: spin, lattice, charge/orbital orders, etc [4–8]. The elementary excitations then depend on a complex set of coupled order parameters with large fluctuations which makes it difficult to underpin their microscopic compositions [9, 10]. Although strong coupling of electronic, magnetic, and lattice degrees of freedom in the manganites is known to lead to coexisting insulating/lattice–distorted/antiferromagnetic (AFM) and metallic/undistorted/ferromagnetic (FM) regions of sizes ∼10–300nm [11], the relevant quasi–particles remain controversial. While electrons localized by Jahn–Teller (JT) lattice distortions dominate the AFM insulating state, some theoretical studies have proposed that the sensitivity to small perturbations leading to CMR phase transition to a FM metallic state is due to coexisting mobile *minority* electrons mediated by classical spin canting [9, 12, 13]. Moreover, while the strong spin–charge coupling should considerably correlate the corresponding *fs* dynamics, the photoexcitation–threshold observed for fs spin generation was absent in the measured optical conductivity [3, 14] and the exact linkage between the two is still elusive. The simultaneous probing of fs spin [3, 15, 16] and charge [17] dynamics may dynamically disentangle degrees of freedom coupled in equilibrium and reveal crucial many–body mechanisms.

This Letter uses fs pump–probe spectroscopy to identify the quasi–particle excitations of $Pr_{0.7}Ca_{0.3}MnO_3$ (PCMO) manganites and quantify their dynamical properties. For this we excite non–equilibrium electron populations close to the insulator energy gap and then probe with fs resolution their effects on both differential reflectivity and magneto–optical responses at 1.55eV and 3.1eV. When pump/probe are *both* tuned at 1.55 eV, we observe a two–step bi–exponential relaxation of charge excitations absent at 3.1eV. These two compo-

Typeset by REVTEX

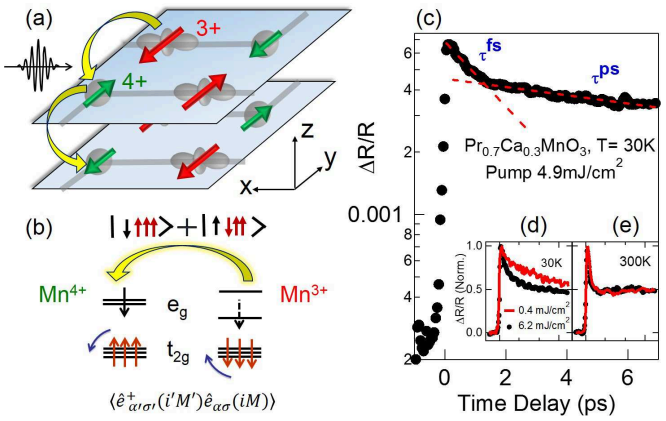

FIG. 1: (Color online) Illustration of (a) fs e–h excitations in CE–AFM/CO/OO ordered manganites and (b) laser–driven off-diagonal bonding–order, via quantum spin canting, of composite fermion quasi–particles (supplementary section). (c): fs–resolved ΔR/R charge dynamics for 1.55eV pump/probe excitation, plotted on a log–scale. Dashed lines highlight two distinct components of bi–exponential decay. (d)-(e): Comparison of normalized ΔR/R for two pump fluences marked at (d) 30K and (e) 300K.

nents, characterized by distinct fast fs ($\tau^{\rm fs}$) and slow ps ($\tau^{\rm ps}$) relaxation times, disappear at higher temperatures. Intriguingly, the ratio of their amplitudes displays a *pump-fluence-threshold* nonlinear dependence that *coincides* with the threshold for *fs* AFM→FM switching. We present calculations indicating *coexistence in a non–equilibrium phase* of fast, mobile, metallic quasi–electrons dressed by *quantum spin fluctuations* ($\tau^{\rm fs}$) with slow, localized polaronic carriers ($\tau^{\rm ps}$). The laser–induced rearrangement of these majority and minority carriers creates a critical non–thermal population of quasi–electrons with strongly–coupled spin–charge degrees of freedom, which drives a simultaneous AFM→FM switching via quantum spin–charge–lattice dynamical coupling.

We consider the CE–AFM–insulator state characterized by coexisting charge (CO), orbital (OO), and magnetic orders [11, 18]. Here, AFM–coupled charge–modulated zig-zag chains have alternating Mn^{3+}/Mn^{4+} ions (CO), FM spins, and JT–distorted lattice sites with populated orbitals pointing along the chain (OO) (Fig. 1(a)). The JT interaction of a localized e_g–electron with its surrounding $Mn^{3+}O_6$ octahedron splits the two degenerate Mn^{3+} states and results in a *polaronic insulator* with populated lower level (JT energy gain E_{JT}) [12, 18]. We study here $Pr_{0.7}Ca_{0.3}MnO_3$ single-crystals grown by the floating–zone method. *All equilibrium phases are insulating*, with CO/OO order below ∼200K and CE–AFM order below ∼140K. A Ti:Sapphire amplifier laser beam, with pulse duration of 35fs and repetition rate of 1kHz, was used in *fs* pump–probe spectroscopy measurements of differential reflectivity $\Delta R/R$, magneto-optical Kerr effect (MOKE, $\Delta\theta_k$), and magnetic circular dichroism (MCD, $\Delta\eta_k$). We thus trace the fs spin and charge dynamics for magnetic field B≤ 0.25T [19].

e_g–electron charge fluctuations are restricted by exchange interaction with the local S=3/2 spins formed by filling all three t_{2g}–orbitals [18, 20] and by suppression of double–occupancies (Mn^{2+}) by the strong local interactions. In classical–spin thermodynamic scenarios, it is energetically favorable for e_g–electrons (spin s=1/2) to move within a single chain so that the spins remain FM–coupled via strong Hund's rule interaction $J_H\mathbf{S}_i\cdot\mathbf{s}_i$. For quantum spins, however, photoelectrons can also hop to sites with anti–parallel t_{2g} spins without magnetic energy cost, illustrated in Fig. 1(b). This is possible by forming quantum states with the same total spin J after flipping t_{2g}–spins via $J_H S_i^{\pm}\cdot s_i^{\mp}$ electron–magnon coupling that leads to quantum spin canting [21] (supplementary section). These ultrafast fluctuations mediate non-local off-diagonal inter-atomic bonding (Fig. 1(b)) and dynamically–entangle neigboring AFM chains, Fig. 1(a), which competes with the AFM surroundings to establish a metastable state (*quantum femtosecond magnetism* [3]). Such FM correlation during the coherently-excited e-hopping has no speed–limit imposed by free energy or spin adiabaticity [12, 22, 23].

Fig.1(c) shows the typical *fs*–resolved $\Delta R(t)/R$ signal at 30K, with *both* pump/probe tuned at 1.55eV. The non–equilibrium quasi–particles excited close to the insulator gap with this relatively high pump fluence ∼4.9 mJ/cm^2 display bi–exponential relaxation, with two distinct relaxation times $\tau^{\rm fs}$∼530fs and $\tau^{\rm ps}$∼5.7ps. This behavior is in striking contrast to the temporal profiles of the low–fluence or high temperature signals (compare the normalized $\Delta R/R$ traces in Figs. 1(d) and (e)). At 30K, the $\tau^{\rm fs}$ component is suppressed for smaller pump fluences of 0.4 mJ/cm^2 (Fig. 1(d)). At 300K, i.e. above the CO/OO transition, all pump fluences give an identical single–exponential decay, with relaxation time much shorter than both $\tau^{\rm fs}$ and $\tau^{\rm ps}$ (Fig. 1(e)). Clearly the charge quasi–particle dynamics strongly depend on both photoexcitation intensity and ground–state order.

Fig. 2 shows a 2D plot of $\Delta R/R$ as function of pump–fluence and probe time delay. The color gradients demonstrate distinct differences, along both axes, between probe frequencies that either couple directly to [1.55 eV, Fig. 2(a)] or decouple from [3.1 eV, Fig. 2(d)] the insulator gap. While at 1.55eV the peak of $\Delta R(t)/R$ shows almost linear fluence–dependence (Fig. 2(b)), at 3.1eV it displays nonlinear saturation (Fig. 2(e)). For 1.55 eV pump/probe, $\Delta R(t)/R$ comes from phase–space–filling by linearly–increasing quasi–particle populations near the insulator gap. Its temporal decay, Fig. 2(c), thus reveals two coexisting quasi–particle populations, with relaxation times $\tau^{\rm fs}$ and $\tau^{\rm ps}$ respectively. For 3.1eV probe/1.55eV pump, $\Delta R(t)/R$ reflects a *fs* increase and saturation of the conductivity, with spectral–

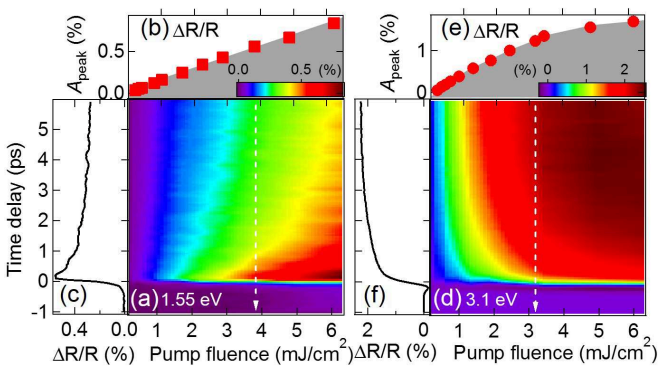

FIG. 2: (Color online) (a)-(c): Ultrafast $\Delta R/R$ dynamics under 1.55eV pump/probe photoexcitation. (a): 2D dependence on pump fluence and time delay at 30K; (b): peak amplitude as function of pump fluence; (c): temporal trace at 3.8mJ/cm^2 marked in (a). (d)-(f): Same $\Delta R/R$ plot as above, but for non–degenerate photoexcitation with 1.55eV pump/3.1eV probe.

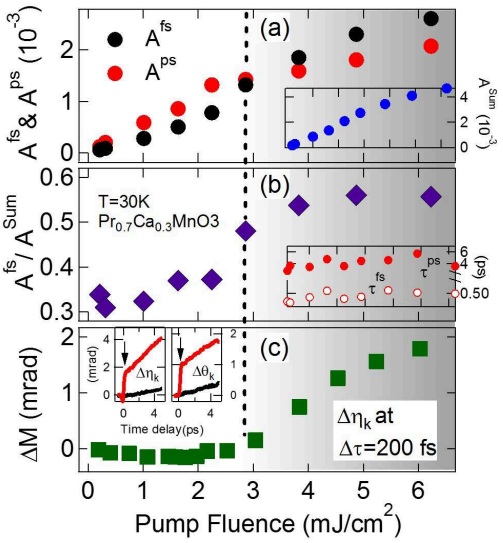

FIG. 3: (Color online) Photoexcitation dependence. (a): Amplitudes of fast component A_{fs} (black dots), slow component A_{ps} (red dots), and A^{sum}= A_{fs}+ A_{ps} (inset). (b): Fraction F=A^{fs}/A^{sum} (blue rhombus) and the two distinct relaxation times (inset). (c): Photoinduced fs magnetization ΔM extracted from $\Delta\eta_k$ at 200fs (green rectangle). Inset: $\Delta\eta_k$ and $\Delta\theta_k$ dynamics for 5.6mJ/cm^2 (red) and 0.8mJ/cm^2 (black). show the same "sudden" magnetization (arrow). All error bars within the markers.

weight transfer to low energies due to a fs pump–induced decrease in the insulator gap. Fig. 2(f) shows a further *ps* increase of $\Delta R(t)/R$, which reflects a slower phonon–related conductivity increase.

We now compare this charge relaxation to the spin dynamics extracted from the fs–resolved magnetic signals. Fig. 3(c) clearly shows threshold for *fs* spin photogeneration above a critical pump–fluence of 2-3mJ/cm^2 where both MOKE and MCD show the *same large quasi–instantaneous jump* (inset). Despite this, Figs. 2(b) and 2(e) show smooth *thresholdless* fluence–dependence of $\Delta R/R$. Disentangling the $\tau^{\rm fs}$ and $\tau^{\rm ps}$ components of $\Delta R(t)/R$ provides the missing link between spin and charge quantum excitations. Fig. 3(a) shows the pump–fluence–dependences of the amplitudes A^{fs} and A^{ps}, via bi–exponential fit, and their sum A^{sum}=A^{fs}+A^{ps} (inset). While A^{sum} appears linear, the two populations A^{fs} and A^{ps} reverse their magnitudes with increasing excitation (Fig. 3(a)). Most intriguingly, a threshold increase of the short–lived ($\tau^{\rm fs}$) minority population is seen in Fig. 3(b) by plotting the fraction F=A^{fs}/A^{sum}. This apparent threshold *coincides* with the threshold for *fs* spin generation in Fig. 3(c), while $\tau^{\rm fs}$ and $\tau^{\rm ps}$ times remain fairly constant (inset of Fig. 3(b)). This direct correlation of AFM→FM switching with critical increasing the proportion of the minority $\tau^{\rm fs}$ population suggests the emergence of a quasi–particle excitation composed of strongly–coupled spin and charge degrees of freedom.

To explore this issue, we model the non–adiabatic [22] spin–charge quantum correlation that dresses *e–h* excitations *during* the fs timescales of coherent light–matter coupling. For this, we solve the quantum–kinetic equations of motion of the spin–dependent density matrix that describes spin/charge non–equilibrium populations and inter–site coherences involving atomic many–body states (supplementary section). In the ground state (Fig. 1(a)), fully–localized JT–polarons (majority carriers) gain lattice energy E_{JT} by populating alternating Mn^{3+} sites (site 1 in Fig.4(a)), with total spin J=S+1/2 and parallel e_g and t_{2g} spins. In the deep–insulating limit of large E_{JT} [12], we neglect electron hopping along FM chains, which does not change the total spin. We focus on quantum correlations between two neigboring AFM atoms in different chains (yellow arrows, Fig. 1(b)), driven by the laser E–field with central frequency $\hbar\omega_p\sim E_{JT}$. The strong charge fluctuations during this fs pump pulse involve hopping of the e_g–electron from the Mn^{3+} atom (ε=$-E_{JT}$) to the JT–undistorted Mn^{4+} atom (ε=0) with *anti–parallel* t_{2g} spin S_z=-S (site 2 in Fig.4(b)). Such virtual [13] and laser–driven fluctuations across the JT gap are faster than the JT distortions for hopping amplitudes $t_0\gg\hbar\omega_{ph}$ [12], so for now our simulation ignores JT displacements (phonon frequency ω_{ph}) to examine the roles of quantum charge/spin fluctuations.

Fig.4 shows all non–equilibrium spin–resolved populations of the two above-discussed sites (Figs. 4(a) and 4(b)) and the z–component of the total t_{2g}–spin, S_z=$S_z(1)$+$S_z(2)$ (Fig. 4(c)). Here $J_H\to\infty$, so an electron can hop between AFM sites *only* by simultaneously flipping t_{2g} spins [20]. This results in correlated spin–charge non–adiabatic dynamics. The bottom panel of Fig.4(a) shows the photoexcited hole popula-

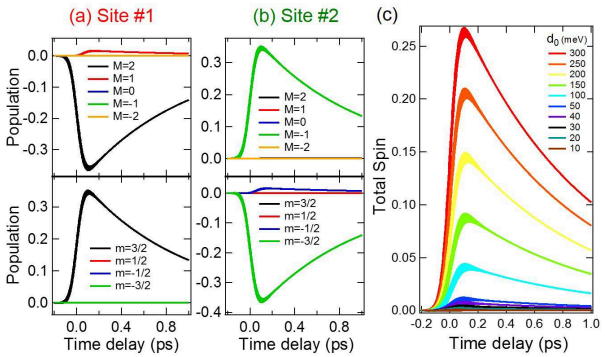

FIG. 4: (Color online) Calculated time–dependence of (a): Spin–resolved Mn^{3+} (upper panel) and Mn^{4+} (lower panel) non–equilibrium populations, (b): Total t_{2g}–spin under different Rabi energies d_0. Here composite fermion populations, T_1=1ps, are riven by e–h photoexcitations with lifetime T_2=50fs.

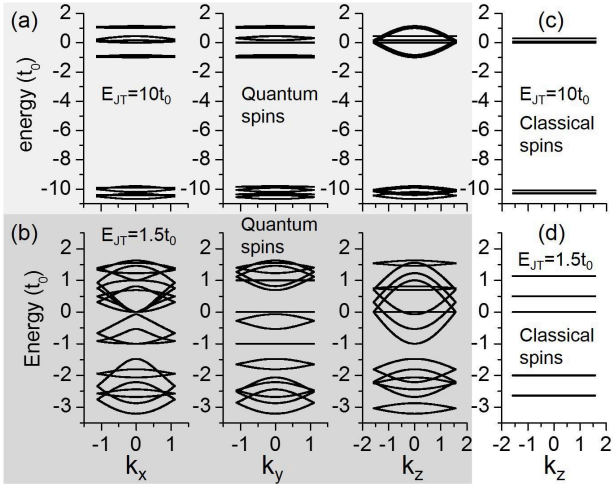

FIG. 5: Calcualted composite–fermion energy dispersions. (a), (b): Quantum Spins, (c), (d): Classical Spins (see text and supplementary section).

tion ($Mn^{3+}\rightarrow Mn^{4+}$ excitation, J_z=S+1/2→S_z=m) of the JT–distorted site 1. Excitation of majority carriers does not change significantly the m=3/2 t_{2g}–spin. In contrast, the minority quasi–electrons ($Mn^{4+}\rightarrow Mn^{3+}$ excitation, S_z=−S→J_z=M) populating site 2 (top panel of Fig.4(b)) have mixed spin due to flipping of the opposite e_g and t_{2g} spins (M=−S+1/2). Such quasi–electron photoexcitations thus induce a quantum dynamics of S_z, which saturates with population inversion (Fig.4(c)). The fluence–dependence of quasi–electron population then naturally correlates with that of the fs spin, as in our experiment (Fig. 3(b)). FM inter–chain correlation arises from this electron dressing by quantum spin fluctuations, driven by fs quantum–spin–canting in the AFM insulating state.

After photoexcitation, the system is thereby left in an excited state with non–thermal populations of two composite–fermion quasi–particles (supplementary section). Subsequent relaxation ($\tau^{\rm fs}$ and $\tau^{\rm ps}$) depends on the quasi–particle energy dispersions, shown in Fig. 5 along three directions: k_x (along the chain), k_y (perpendicular to the chain, along the same plane), and k_z (perpendicular to the plane). We considered one–electron excitations of the CE–type CO/OO/AFM ordered periodic state [24] without spin–canting (supplementary section). Fig. 5 compares our quantum spin results to the classical limit $S\rightarrow\infty$, where we reproduce previous results [11, 25]. For classical spins, an *adiabatic description* applies: the diagonalized electronic Hamiltonian describes energy bands that depend on *fixed* local spin and JT–distortion patterns [11, 12]. For large J_H, the frozen CE–AFM spin pattern then only allows photoelectron dispersion along a single FM chain [20]. For quantum spins, however, photoelectrons move by *simultaneously* deforming local spins (e.g. electron–magnon coupling [21]). They decrease the insulator gap, Fig. 5, by hopping *between* chains parallel (k_y) or perpendicular (k_z) to the plane (Fig. 1(a)) [26].

For large E_{JT}, Fig. 5(a) demonstrates anisotropic quasi–particle dispersions with energies close to the Mn^{3+} (ε=0) and Mn^{4+} (ε=−E_{JT}) localized levels. CO suppresses electron hopping *along the plane* due to the JT energy gap between all neigboring sites, so dispersion along k_x and k_y is small. For classical spins, charge carriers are fairly localized in *all three* directions, as neigboring planes have opposite spins. For quantum spins, however, inter–plane hopping *between JT–undistorted sites* (Fig. 1(a)) becomes possible by deforming the ground state AFM spins. This results in large dispersion along k_z, only for the spin–dressed conduction quasi–electrons close to ε=0 (Fig. 5(a)). As in Fig. 4, polaronic holes do not deform strongly the parallel background spins, so the valence band dispersion in Fig. 5(a), close to ε=−E_{JT}, is small. Relaxation across the large insulator gap is suppressed, so photoexcitation creates non–equilibrium e and h populations *with two very different chemical potentials and spin properties*. A critical density of quasi–electrons in the dispersive conduction band leads to *anisotropic metallic properties* and global conductivity. The (FM) spin–canting responsible for this mobility dominates over JT distortion in determining the free energy change [12]. In contrast, holes have weak dispersion, small Fermi energy, and localize by relaxing JT distortions to gain elastic energy [12]. The differences between classical and quantum spins become most pronounced as E_{JT} decreases to values reasonable for some manganites (Figs. 5(b) and 5(d)). Quantum spin fluctuations can then overcome JT confinement to enhance delocalization of *both* e and h quasi–particles in all three directions and rapidly close the charge energy gap. Decreasing E_{JT} favors an insulator–to–metal transition [13] for quantum

spins, which may explain why classical spin calculations require critical magnetic fields for CMR phase transition much larger [26] than experiment [12]. Note that the presence of lattice deformations [8, 27] can work cooperatively with the proposed electronic fluctuation mechanism to decrease E_{JT} and further enhance the above effects.

In summary, by simultaneously tracing the *fs* dynamics of charge and spin excitations, we provide solid evidence that the properties of CMR manganites are governed by the coexistence of two very different quasi–particles: metallic quasi–electrons dressed by quantum spin fluctuations and JT polarons. Femtosecond coherent nonlinear excitation controls a "sudden" AFM→FM switching in the insulating phase, coincident with majority/minority carrier reversal and closing of the JT energy gap by quantum spin fluctuations.

This work was supported by the National Science Foundation Contract No. DMR-1055352 (ultrafast laser spectroscopy). The computational studies were supported by the European Union's Seventh Framework Programme (FP7-REGPOT-2012-2013-1) under grant agreement No. 316165, and by the EU Social Fund and National resources through the THALES program NANOPHOS.

[1] D. S. Chemla, and J. Shah, Nature **411**, 549 (2001).
[2] V. M. Axt, and S. Mukamel, Rev. Mod. Phys. **70**, 145 (1998).
[3] T. Li, A. Patz, L. Mouchliadis, J. Yan, T. A. Lograsso, I. E. Perakis, and J. Wang, Nature **496**, 69 (2013).
[4] Y.M. Sheu, S.A. Trugman, L. Yan, J. Qi, Q.X. Jia, A.J. Taylor, and R.P. Prasankumar, Phys. Rev. X **4**, 021001 (2014).
[5] H. Ichikawa, *et. al.*, Nature Mat., **10**, 2929 (2011).
[6] M.Fiebig, K. Miyano, Y Tomioka, and Y Tokura, Science **280**, 1925 (1998).
[7] D. Polli, M. Rini, S. Wall, R. W. Schoenlein, Y. Tomioka, Y. Tokura, G. Cerullo, and A. Cavalleri, Nature Mat. **6**, 643 (2007).
[8] M. Rini, R. Tobey, N. Dean, J. Itatani, Y. Tomioka, Y. Tokura, R. W. Schoenlein, and A. Cavalleri, Nature **449**, 72 (2007).
[9] G. C. Milward, M. J. Calderón, and P. B. Littlewood, Nature **433**, 607 (2005).
[10] A. Patz, T. Li, S. Ran, R. M. Fernandes, J. Schmalian, S. L. Budko, P. C. Canfield, I. E. Perakis, and J. Wang, Nat. Commun. **5**, 3229 (2014).
[11] E. Dagotto, T. Hotta, and A. Moreo, Phys. Rep. **344**, 1 (2001).
[12] V. Ramakrishnan, H. R. Krishnamurthy, S. R. Hassan, and G. Venketeswara Pai, Phys. Rev. Lett. **92**, 157203 (2004); O. Cepas, H. R. Krishnamurthy, and T. V. Ramakrishnan, Phys. Rev. B **73**, 035218 (2006).
[13] T. V. Ramakrishnan, J. Phys. Condens. Matter **19**, 125211 (2007).
[14] Y. Okimoto, H. Matsuzaki, Y. Tomioka, I. Kezsmarki, T. Ogasawara, M. Matsubara, H. Okamoto, and Y. Tokura, J. Phys. Soc. Jpn. **76**, 043702 (2007)
[15] J. Bigot, M. Vomir, and E. Beaurepaire, Nat. Phys. **5**, 515(2009)
[16] R. R. Subkhangulov, A. B. Henriques, P. H. O. Rappl, E. Abramof, Th. Rasing, and A. V. Kimel Sci. Rep. **4** 4368 (2014)
[17] G.D. Sanders, C.J. Stanton, J. Wang, J. Kono, A. Oiwa, H. Munekata, Phys. Rev. B, **72**, 04245302 (2005)
[18] Y. Tokura and N. Nagaosa, Science **288**, 462 (2000).
[19] Our magnetic field is at least one order of magnitude smaller than the critical field needed for CMR transition.
[20] P. W. Anderson and H. Hasegawa, Phys. Rev. **100**, 675 (1955); P.–G. de Gennes, Phys. Rev. **118**, 141 (1960).
[21] M. D. Kapetanakis and I. E. Perakis, Phys. Rev. Lett. **101**, 097201 (2008); Phys. Rev. B **78**, 155110 (2008).
[22] The commonly–used adiabatic approximation assumes spin dynamics slower than electron dynamics, in which case an effective spin Hamiltonian with spin–exchange interaction mediated by fast electrons has meaning. It does not apply to the quantum spin–canting dynamics here where inter–atomic e_g–electron hopping simultaneously flip the t_{2g}–electron localized spins.
[23] J.H. Mentink, and M. Eckstein, Phys. Rev. Lett. **113**, 057201 (2014).
[24] Our unit cell has 16 sites with alternating Mn^{3+}(JT–distorted, polaronic state, orbital points along the chain) and Mn^{4+}(undistorted, two degenerate orbitals) atoms, 4 sites per zig–zag chain, two AFM chains per plane, and two AFM planes with identical charge/lattice/orbital configurations (Fig. 1(a)). Spin–canting angle θ=0.
[25] J. van der Brink, G. Khaliullin, and D. Khmoskii, Phys. Rev. Lett. **83**, 5118 (1999).
[26] While a ground state spin–canting angle θ also leads to electron mobility along k_z, even for classical adiabatic spins, a k_z–dispersion similar to Fig. 5 (S=3/2 quantum spins with θ=0) requires a very large θ of few tens of degrees (θ=90^o corresponds to full FM order without spin dynamics). Such spin–canting requires a very large external magnetic field, much larger than in CMR experiments. Quantum spin fluctuations, which we control here via laser–induced fs e–h coherence, can explain this discrepancy and greatly enhance the sensitivity of fs AFM→FM phase transitions far from equilibrium.
[27] H. Y. Hwang, S-W. Cheong, P. G. Radaelli, M. Marezio, and B. Batlogg, Phys. Rev. Lett. **75**, 914 (1995)

SUPPLEMENTARY INFORMATION

COMPOSITE FERMION QUASI–PARTICLES

Here we summarize the formalism used to describe the dynamical coupling of spin and charge excitations in the strong–coupling insulating limit. Our observations of ultrafast electron hopping correlated with fs spin dynamics suggest that this is a key many–body mechanism in manganites. Classical spin scenarios assume an adiabatic approximation of electrons scattering off a frozen spin configuration [12]. The effective inter–atomic hopping amplitude then decreases with increasing angle between

the local spins [11, 12, 20] and electron hopping is suppressed by AFM spin alignment. For the CE–AFM reference state, this results in electronic confinement within one–dimensional FM chains with parallel e_g and t_{2g} spins [11, 25]. Spin dynamics directly correlated with *simultaneous* photoelectron femtosecond motion is impossible within the classical spin adiabatic approximation. We therefore had to turn to non–adiabatic *quantum spin* scenarios in order to explain our observation of correlated simultaneous spin–charge femtosecond dynamics.

Our proposed theory addresses the following issues: (i) local interactions well–exceed the kinetic energy and restrict the population of certain atomic configurations, (ii) while here strong on–site interactions result in an insulating ground state, the spin properties are still determined by electron hopping between different atoms [13]. In equilibrium, virtual inter–atomic electronic fluctuations across the JT insulator energy gap lead to a FM exchange coupling [12, 13]. During fs laser excitation, coherent e–h excitations are driven across the JT gap and controlled via optical field Rabi energy and central frequency. Here we show that these driven fast charge fluctuations result in non–equilibrium "sudden" FM correlation, (iii) our experimental results indicate that the coherent charge excitations bring the system away from equilibrium while *simultaneously* exciting the spin degrees of freedom. This observation suggests that non–adiabatic spin dynamics during femtosecond electronic timescales is key for explaining our experiment, while the classical spin adiabatic approximation assumes independent spin and charge degrees of freedom [11, 12]. Below we introduce composite fermion quasi–particles with coupled spin–charge degrees of freedom.

Since the strong interactions are local, we start with atomic states that diagonalize the Hund's rule and JT interactions at given atom i. Each atom can be populated by 0 or 1 mobile (e_g) electrons, since occupancy by two e_g electrons (Mn^{2+} configurations) is suppressed, e.g. by large Hubbard–U repulsion. The atomic states with a single e_g electron are

$$|i\alpha M\rangle \;=\; \sqrt{\frac{S+M+\frac{1}{2}}{2S+1}}\; c^{\dagger}_{i\alpha\uparrow}\,|i,M-\frac{1}{2}\rangle + \sqrt{\frac{S-M+\frac{1}{2}}{2S+1}}\; c^{\dagger}_{i\alpha\downarrow}\,|i,M+\frac{1}{2}\rangle, \qquad (1)$$

where $c^{\dagger}_{i\alpha\sigma}$ adds a spin–σ e_g electron in orbital state α and $|iS_z\rangle$, $S_z{=}{-}S,\cdots,S$, are $S{=}3/2$ local (t_{2g}) spin states for given lattice displacement at site i. The above $J{=}S{+}1/2$, $M{=}{-}J,\cdots,J$ states are characterized by the eigenvalues (J,M) of the total mobile (e_g) plus local (t_{2g}) spin. For $J_H{\to}\infty$, the population of $J{=}S{-}1/2$ states is suppressed. For $M{=}J{=}S{+}1/2$, the itinerant and local spins are parallel, as for classical spins. The quantum spin dynamics discussed in the main text arises mostly from $M{=}S{-}1/2$ atomic states Eq.(1), with mixed spin due to the off–diagonal interaction $J_H S_i^{\pm}{\cdot}s_i^{\mp}$.

In the limit of strong correlation, we describe local excitations in terms of transitions between the above atomic many–body states $|ia\rangle$, created by the "Hubbard operators" $|ia\rangle\langle ib|$. On–site excitations that conserve the total number of electrons are created by the operators

$$\hat{X}_i(\alpha M;\alpha' M') = |i\alpha M\rangle\langle i\alpha' M'|\;,\; \hat{X}_i(m;m') = |im\rangle\langle im'|. \qquad (2)$$

In the limit of large Hubbard–U and Hund's rule magnetic exchange interactions, the local (t_{2g}) spin z–component $S_z(i)$ at site i is expressed as

$$S_z(i) = \sum_{m=-S}^{S} m\,\rho_i(m) + \sum_{M=-S-\frac{1}{2}}^{S+\frac{1}{2}} M\,\frac{S}{S+\frac{1}{2}}\sum_{\alpha}\rho_i^{\alpha}(M), \qquad (3)$$

where the diagonal density matrix elements

$$\rho_i(m) = \langle \hat{X}_i(m,m)\rangle = \langle |im\rangle\langle im|\rangle$$
$$\rho_i^{\alpha}(M) = \langle \hat{X}_i(\alpha M;\alpha M)\rangle = \langle |i\alpha M\rangle\langle i\alpha M|\rangle, \qquad (4)$$

$m{=}{-}S,\cdots,S$ and $M{=}{-}J,\cdots,J$, give the populations of the empty and singly–occupied atomic configurations. Their equations–of–motion couple off–diagonal density matrix elements that describe linear superpositions of quantum states in *two different* atoms (e–h coherence). We describe such e–h coherence for strong on–site interactions by first introducing "composite fermion" local excitations with fixed *total spin* $J_z{=}\sigma/2$. These quasi–electron charge excitations are created by Hubbard operators that change the number of electrons on a given atom by one via $Mn^{4+}{\to}\,Mn^{3+}$ transitions between the many–body states that diagonalize the strong spin, charge, and lattice on–site interactions:

$$\hat{e}^{\dagger}_{\alpha\sigma}(iM) = |i\alpha M\rangle\langle i, M-\frac{\sigma}{2}|\;,\; M=-J,\cdots,J. \qquad (5)$$

The e–h coherence is characterized by the off–diagonal density matrix elements $\langle \hat{e}^{\dagger}_{\alpha'\sigma'}(i'M')\,\hat{e}_{\alpha\sigma}(iM)\rangle$, which are defined in terms of composite fermions. Delocalized excitations in a periodic lattice of atoms located at positions (i,R_i), where i now labels the different atoms in a single unit cell and R_i is the periodic lattice vector that labels the different unit cells, are described by transforming to k–space using the Bloch theorem:

$$\hat{e}^{\dagger}_{k\sigma}(i\alpha M) = \frac{1}{\sqrt{N}}\sum_{R_i} e^{ikR_i}\,\hat{e}^{\dagger}_{\alpha\sigma}(iR_iM), \qquad (6)$$

where N is the number of unit cells and k the wavevector.

Composite fermions obey the non–canonical anti–commutation relations

$$[\hat{e}^{\dagger}_{\alpha'\sigma'}(i'M'),\hat{e}_{\alpha\sigma}(iM)]_+ = \delta_{ii'}\ \left[\delta_{M',M+\frac{\sigma'-\sigma}{2}}\ \hat{X}_i(\alpha'M';\alpha M)+\delta_{M',M}\ \delta_{\alpha,\alpha'}\ \hat{X}_i(M-\frac{\sigma}{2},M'-\frac{\sigma'}{2})\right]. \quad (7)$$

The difference from fermion anti–commutator is often referred to as "kinematic interaction" and comes from the restriction, due to on–site interactions exceeding the kinetic energy, in the populations of individual atoms where the electron is allowed to hop. For example, strong Hubbard repulsion and Hund's rule interactions suppress doubly–occupied and $J{=}S{-}1/2$ atomic configurations during electron motion. We thus project the bare electron operators onto the subspace of the low–energy populated states Eq.(1):

$$\hat{e}^{\dagger}_{\alpha\sigma}(i)=\sum_M F_\sigma(M)\ \hat{e}^{\dagger}_{\alpha\sigma}(iM), \quad (8)$$

where the Glebsch–Gordan coefficients

$$F_\sigma(M)=\sqrt{\frac{S+\frac{1}{2}+\sigma M}{2S+1}} \quad (9)$$

arise from the conservation of the total spin $\mathbf{J}$. The projected time–dependent many–body Hamiltonian that describes the laser–excited system has the form

$$H(t)=\sum_i\sum_{\alpha M} E_i(\alpha M)\,\hat{X}_i(\alpha M;\alpha M) + \sum_i\sum_m E_i(m)\,\hat{X}_i(m,m)+H_{hop}(t). \quad (10)$$

The first two terms diagonalize exactly the many–body atomic Hamiltonian that includes all onsite interactions, with eigenvalues $E_i(\alpha M)$ (Mn^{3+}) and $E_i(m)$ (Mn^{4+}). The eigenvalues $E_i(\alpha M)$ of states with a single e_g electron depend on the lattice displacement at site i due to electron–phonon interaction with the local vibrational (JT) modes. While the above two terms dominate in the insulating limit, inter–site electron hopping is allowed via fast charge fluctuations, virtual [12, 13] or driven by the time–dependent laser E–field:

$$H_{hop}(t)=-\sum_{ii'}\sum_\sigma\sum_{\alpha\alpha'}V_{\alpha\alpha'}(i-i')\left[\cos\left(\frac{\theta_i-\theta_{i'}}{2}\right)\ \hat{e}^{\dagger}_{\alpha\sigma}(i)\,\hat{e}_{\alpha'\sigma}(i')+\sigma\ \sin\left(\frac{\theta_i-\theta_{i'}}{2}\right)\ \hat{e}^{\dagger}_{\alpha\sigma}(i)\,\hat{e}_{\alpha'-\sigma}(i')\right]. \quad (11)$$

For tight–binding Hamiltonians, the hopping amplitude between sites r_i and r_j is modified by the laser (vector potential $\mathbf{A}$(t)) as described by the Peierls substitution

$$V_{\alpha\alpha'}(j-i)=t_{\alpha\alpha'}(j-i)\exp[-ie\mathbf{A}(t)\cdot(r_j-r_i)/\hbar c], \quad (12)$$

where $t_{\alpha\alpha'}$ are the tight–binding parameters. We decompose this hopping amplitude into equilibrium and laser–induced parts, $V_{\alpha\alpha'}(j-i)=t_{\alpha\alpha'}+\Delta V_{\alpha\alpha'}(t)$, where for our typical pump intensities

$$\Delta V_{\alpha\alpha'}(i-j)\approx d_0(t)\ \frac{t_{\alpha\alpha'}(i-j)}{\hbar\omega_p}. \quad (13)$$

The time–dependence of the Rabi energy d_0(t)$=eE(t)a$, where a is the lattice spacing, is determined by the amplitude of the laser field $\propto e^{-t^2/t_p^2}$. $\hbar\omega_p$ is the pump central frequency and we consider t_p=100fs.

In Eq.(11), the spin–canting angles θ_i characterize the reference (equilibrium) state and define the spin background within the adiabatic approximation (we assume zero polar angles). These angles describe the tilt of the local z–axis at site i, defined by the direction of the equilibrium spins, with respect to the laboratory z–axis. In the calculations presented here, we assume AFM ground state, so $\theta_i{=}0$ at spin–$\uparrow$ sites and $\theta_i{=}\pi$ at spin–$\downarrow$ sites. For $\sigma{=}\uparrow$, the first term on the rhs of Eq.(11) describes the usual coherent electron hopping amplitude [11, 12, 20], which is maximum for parallel spins $\theta_i{=}\theta_{i'}$. For $\sigma{=}\downarrow$, this term describes electron hopping accompanied by simultaneous spin–flips on both initial and final sites. The second term describes the electron–magnon interaction [21] in the strong–coupling limit, which allows an electron to hop between two sites with opposite (AFM) spins.

QUANTUM KINETICS OF SPIN–CHARGE COUPLING: EQUATIONS OF MOTION

In this section we summarize the quantum kinetic density matrix equations of motion that we use to describe the simultaneous spin and charge excitation while the laser pulse interacts with the material (coherent tempo-

ral regime). These equations are derived by using the time–dependent Hamiltonian Eq.(10). The time evolution of the spin–dependent atomic populations (diagonal density matrix elements) is described as follows:

$$i\partial_t \rho_i^{\alpha}(M) = 2\,Im\,\frac{1}{N}\sum_{k'}\sum_{l\alpha'} V_{\alpha'\alpha}^{k'}(l-i)\sum_{\sigma'=\pm 1} F_{\sigma'}(M)\times$$
$$\left[\cos\left(\frac{\theta_l-\theta_i}{2}\right)\langle \hat{e}^{\dagger}_{k'\sigma'}(l\alpha')\,\hat{e}_{k'\sigma'}(i\alpha M)\rangle - \sigma'\sin\left(\frac{\theta_l-\theta_i}{2}\right)\langle \hat{e}^{\dagger}_{k'-\sigma'}(l\alpha')\,\hat{e}_{k'\sigma'}(i\alpha M)\rangle\right] \quad (14)$$

determines the population of atomic many–body configurations with a single e_g–electron and

$$\partial_t \rho_i(m) = -2\,Im\,\frac{1}{N}\sum_{k'}\sum_{l\alpha'\alpha} V_{\alpha'\alpha}^{k'}(l-i)\sum_{\sigma'=\pm 1} F_{\sigma'}(m+\frac{\sigma'}{2})\times$$
$$\left[\cos\left(\frac{\theta_l-\theta_i}{2}\right)\langle \hat{e}^{\dagger}_{k'\sigma'}(l\alpha')\,\hat{e}_{k'\sigma'}(i\alpha,m+\frac{\sigma'}{2})\rangle - \sigma'\,\sin\left(\frac{\theta_l-\theta_i}{2}\right)\langle \hat{e}^{\dagger}_{k'-\sigma'}(l\alpha')\,\hat{e}_{k'\sigma'}(i\alpha,m+\frac{\sigma'}{2})\rangle\right] \quad (15)$$

determines the population of atomic configurations with empty e_g orbitals (t_{2g} spin only). In the above equations, we introduced the Fourier–transform of the time–dependent hopping amplitude $V_{\alpha\beta}$, Eq.(12), assuming a periodic system with different atoms i and j per unit cell:

$$V_{\alpha\beta}^{k}(i-j) = \sum_{R} V_{\alpha\beta}(R+i-j)\,e^{-ikR}. \quad (16)$$

The above population equations of motion are *exact* in the limit $J_H, U\to\infty$. They describe the dynamical coupling of any given atom i to the rest of the lattice, driven by $H_{hop}(t)$ Eq.(11). This dynamics is characterized by the time–dependent inter–atomic e–h coherences $\langle \hat{e}^{\dagger}_{k'\pm\sigma'}(l\alpha')\,\hat{e}_{k'\sigma'}(i\alpha,m+\frac{\sigma'}{2})\rangle$, Fig. 1(b), of composite fermion excitations (rather than bare–electrons as with e–h excitations in weakly correlated systems [1, 2]). These coherences characterize transient superpositions of spin–dependent many–body atomic states in the pair of atoms i and l in the unit cell. Of main interest here is the laser–driven time–dependent coherence across the JT insulator gap, between JT–distorted sites and undistorted sites. In real space, the dynamics of inter–atomic coupling is determined by the following (exact) equations of motion:

$$i\partial_t\langle \hat{e}^{\dagger}_{\beta\bar{\sigma}}(j)\,\hat{e}_{\alpha\sigma}(iM)\rangle - [\varepsilon_{\alpha\sigma}(i)-\varepsilon_{\beta\bar{\sigma}}(j)]\,\langle \hat{e}^{\dagger}_{\beta\bar{\sigma}}(j)\,\hat{e}_{\alpha\sigma}(iM)\rangle$$
$$= \sum_{l\sigma'}\sum_{\alpha'\beta'} V_{\alpha'\beta'}(l-j)\,\cos\left(\frac{\theta_l-\theta_j}{2}\right)\,\langle [\hat{e}^{\dagger}_{\beta\bar{\sigma}}(j),\hat{e}_{\beta'\sigma'}(j)]_+\,\hat{e}^{\dagger}_{\alpha'\sigma'}(l)\,\hat{e}_{\alpha\sigma}(iM)\rangle$$
$$-\sum_{l\sigma'}\sum_{\alpha'\beta'} V_{\alpha'\beta'}(i-l)\,\cos\left(\frac{\theta_l-\theta_i}{2}\right)\,\langle \hat{e}^{\dagger}_{\beta\bar{\sigma}}(j)\,\hat{e}_{\beta'\sigma'}(l)\,[\hat{e}^{\dagger}_{\alpha'\sigma'}(i),\hat{e}_{\alpha\sigma}(iM)]_+\,\rangle$$
$$+\sum_{l\sigma'}\sum_{\alpha'\beta'} V_{\alpha'\beta'}(l-j)\,\sigma'\,\sin\left(\frac{\theta_l-\theta_j}{2}\right)\,\langle [\hat{e}^{\dagger}_{\beta\bar{\sigma}}(j),\hat{e}_{\beta'-\sigma'}(j)]_+\,\hat{e}^{\dagger}_{\alpha'\sigma'}(l)\,\hat{e}_{\alpha\sigma}(iM)\rangle$$
$$+\sum_{l\sigma'}\sum_{\alpha'\beta'} V_{\alpha'\beta'}(i-l)\,\sigma'\,\sin\left(\frac{\theta_l-\theta_i}{2}\right)\,\langle \hat{e}^{\dagger}_{\beta\bar{\sigma}}(j)\,\hat{e}_{\beta'-\sigma'}(l)\,[\hat{e}^{\dagger}_{\alpha'\sigma'}(i),\hat{e}_{\alpha\sigma}(iM)]_+\rangle, \quad (17)$$

where we introduced the many–body excitation energies

$$\varepsilon_{\alpha\sigma}(i) = E_i(\alpha M) - E_i(M-\frac{\sigma}{2}). \quad (18)$$

Eq.(17) treats non–adiabatic quantum spin dynamics during the fast electronic motion and couples dynamically spin and charge excitations.

Coherence between many–body states across the Mott–Hubbard insulator gap couples the two Hubbard bands and is at the heart of the insulator–to–metal phase transition. Here, Eq.(17) was derived in the limit $U, J_H \to \infty$, where the finite insulator energy gap arises between JT–distorted and undistorted sites. The laser excitation drives femtosecond non–equilibrium coherence across this JT insulator gap. The differences from the familiar equations of motion for e–h coherence in weakly–correlated systems [1, 2] arise from the deviation of the *composite fermion* anti–commutators $[\hat{e}^\dagger_{\alpha'\sigma'}(i), \hat{e}_{\alpha\sigma}(iM)]_+$ from fermion behavior (kinematic interaction). This effect of strong local correlations couples two– and four–particle density matrices, leading to a many–body hierarchy. The spin–dependent composite fermion operators $\hat{e}^\dagger_{\alpha\sigma}(iM)$, Eq. (5), not only project–out double–occupancy of any site, but also distinguish between many–body atomic populations with different *total spin*, after diagonalizing exactly the magnetic exchange interaction that mixes individual spins. σ labels the *total spin* of the many–body excitation $|iM - \frac{\sigma}{2}\rangle \to |i\alpha M>$ created by $\hat{e}^\dagger_{\alpha\sigma}(iM)$ and coincides with the bare electron spin only if we neglect local spin excitation during electronic hopping, as in the classical spin adiabatic approximation. Eq.(17) couples $\pm\sigma$ local excitations in sites i and j with different equilibrium spin orientations, $\theta_i \neq \theta_j$, and describes electron motion in AFM systems.

To truncate the hierarchy of equations of motion, we factorize the four–particle density matrices of *composite fermions* (rather than bare electrons) in Eq.(17) similar to the Gutzwiller wavefunction approximation in infinite dimensions. In particular, we use the factorization

$$\langle [\hat{e}^\dagger_{\beta\bar{\sigma}}(j), \hat{e}_{\beta'\sigma'}(j)]_+ \, \hat{e}^\dagger_{\alpha'\sigma'}(l) \, \hat{e}_{\alpha\sigma}(iM)\rangle = \langle [\hat{e}^\dagger_{\beta\bar{\sigma}}(j), \hat{e}_{\beta'\sigma'}(j)]_+\rangle \langle \hat{e}^\dagger_{\alpha'\sigma'}(l) \, \hat{e}_{\alpha\sigma}(iM)\rangle, \tag{19}$$

where $j \neq l, i$, which after using total spin conservation transforms Eq.(17) to

$$\begin{aligned}
&i\partial_t \langle \hat{e}^\dagger_{\beta\bar{\sigma}}(j) \, \hat{e}_{\alpha\sigma}(iM)\rangle - [\varepsilon_{\alpha\sigma}(i) - \varepsilon_{\beta\bar{\sigma}}(j)] \, \langle \hat{e}^\dagger_{\beta\bar{\sigma}}(j) \, \hat{e}_{\alpha\sigma}(iM)\rangle \\
&= \sum_l \sum_{\alpha'\beta'} V_{\alpha'\beta'}(l-j) \, \langle [\hat{e}^\dagger_{\beta\bar{\sigma}}(j), \hat{e}_{\beta'\bar{\sigma}}(j)]_+\rangle \, \langle \left[\cos\left(\frac{\theta_l - \theta_j}{2}\right) \hat{e}^\dagger_{\alpha'\bar{\sigma}}(l) - \bar{\sigma} \sin\left(\frac{\theta_l - \theta_j}{2}\right) \hat{e}^\dagger_{\alpha'-\bar{\sigma}}(l) \right] \hat{e}_{\alpha\sigma}(iM)\rangle \\
&- \sum_l \sum_{\alpha'\beta'} V_{\alpha'\beta'}(i-l) \, \langle [\hat{e}^\dagger_{\alpha'\sigma}(i), \hat{e}_{\alpha\sigma}(iM)]_+\rangle \, \langle \hat{e}^\dagger_{\beta\bar{\sigma}}(j) \left[\cos\left(\frac{\theta_l - \theta_i}{2}\right) \hat{e}_{\beta'\sigma}(l) - \sigma \sin\left(\frac{\theta_l - \theta_i}{2}\right) \hat{e}_{\beta'-\sigma}(l) \right] \rangle.
\end{aligned} \tag{20}$$

In a periodic system, we can take advantage of the Bloch theorem and Fourier–transform the above equation to k–space by using Eq.(6). We consider for simplicity two neigboring atoms in the unit cell, $i \neq j$, and neglect the energy dispersion $V^k_{\alpha\beta}(0)$ in the insulating limit. We then obtain in k–space

$$\begin{aligned}
&i\partial_t \langle \hat{e}^\dagger_{k\bar{\sigma}}(j\beta) \, \hat{e}_{k\sigma}(i\alpha M)\rangle - [\varepsilon_{\alpha\sigma}(i) - \varepsilon_{\beta\bar{\sigma}}(j)] \, \langle \hat{e}^\dagger_{k\bar{\sigma}}(j\beta) \, \hat{e}_{k\sigma}(i\alpha M)\rangle \\
&= \left[\delta_{\sigma,\bar{\sigma}} \cos\left(\frac{\theta_i - \theta_j}{2}\right) + \sigma\delta_{\sigma,-\bar{\sigma}} \, \sin\left(\frac{\theta_i - \theta_j}{2}\right) \right] \times \\
&\sum_{\alpha'\beta'} V^k_{\alpha'\beta'}(i-j) \, \left[\langle [\hat{e}^\dagger_{\beta\bar{\sigma}}(j), \hat{e}_{\beta'\bar{\sigma}}(j)]_+\rangle \, \langle \hat{e}^\dagger_{k\sigma}(i\alpha') \, \hat{e}_{k\sigma}(i\alpha M)\rangle - \langle [\hat{e}^\dagger_{\alpha'\sigma}(i), \hat{e}_{\alpha\sigma}(iM)]_+\rangle \, \langle \hat{e}^\dagger_{k\sigma}(j\beta) \, \hat{e}_{k\sigma}(j\beta')\rangle \right].
\end{aligned} \tag{21}$$

In the above equation, local correlations described by the composite fermion anti–commutators modify the coherence and populations of the delocalized carriers. In the deep insulating limit $t \ll E_{JT}$, we further simplify the problem by neglecting long–range coherence between different unit cells and approximate

$$\langle \hat{e}^\dagger_{k\bar{\sigma}}(i\beta) \hat{e}_{k\sigma}(i\alpha M)\rangle \approx \delta_{\sigma\bar{\sigma}} \, F_\sigma(M) \, \rho^{\beta\alpha}_i(M) = \frac{1}{N} \sum_{k'} \langle \hat{e}^\dagger_{k'\bar{\sigma}}(i\beta) \hat{e}_{k'\sigma}(i\alpha M)\rangle. \tag{22}$$

After using Eqs.(7) and (8) to express the composite fermion anti–commutators in terms of the local density matrix,

$$\langle [\hat{e}^\dagger_{\alpha\sigma'}(i'), \hat{e}_{\alpha\sigma}(i)]_+\rangle = \delta_{ii'}\delta_{\sigma\sigma'} \left[\sum_{M=-S-\frac{1}{2}}^{S+\frac{1}{2}} F^2_\sigma(M) \, \rho^\alpha_i(M) + \sum_{m=-S}^{S} F^2_\sigma(m + \frac{\sigma}{2}) \, \rho_i(m) \right], \tag{23}$$

Eq.(21) reduces to

$$\begin{aligned}
&i\partial_t \langle \hat{e}^\dagger_{k\bar{\sigma}}(j\beta) \, \hat{e}_{k\sigma}(i\alpha M)\rangle - [\varepsilon_{\alpha\sigma}(i) - \varepsilon_{\beta\bar{\sigma}}(j)] \, \langle \hat{e}^\dagger_{k\bar{\sigma}}(j\beta) \, \hat{e}_{k\sigma}(i\alpha M)\rangle = V^k_{\alpha\beta}(i-j) \, F_\sigma(M) \times \\
&\left[\delta_{\sigma,\bar{\sigma}} \cos\left(\frac{\theta_i - \theta_j}{2}\right) + \sigma\delta_{\sigma,-\bar{\sigma}} \, \sin\left(\frac{\theta_i - \theta_j}{2}\right) \right] \sum_{M'} F^2_{\bar{\sigma}}(M') \left[\rho^\alpha_i(M) \, \rho_j(M' - \frac{\bar{\sigma}}{2}) - \rho_i(M - \frac{\sigma}{2}) \, \rho^\beta_j(M') \right].
\end{aligned} \tag{24}$$

The population product on the rhs describes population–inversion nonlinearity and nonlinear saturation. Eqs.(14), (15), and (24) provide a closed system of equations of motion used to obtain the time–dependent results of Fig. 4. Eq.(24) treats short–range coherence between nearest–neigbor atoms with different JT disotrions, which form "quantum dimers" due to coherent coupling by the laser field across E_{JT}. This provides a first correction to the atomic limit. The quasi–equilibrium state of the system can be obtained by solving the above equations in the adiabatic limit, by setting ∂_t=0. For classical spins, this recovers the equilibrium results of Ref. [12, 13], where a population–dependent FM exchange interaction was obtained from virtual charge fluctuations between neigboring atoms with different JT distortions.

COMPOSITE–FERMION QUASI–PARTICLE ENERGY DISPERSIONS FOR CE–AFM INSULATOR REFERENCE STATE

In this section, we summarize the calculation of the composite–fermion excitation energy dispersion for a CE–AFM/CO/OO reference state with coupled spin, charge, lattice, and orbital long–range orders. For this we consider the coherent coupling of the $Mn^{4+}\rightarrow Mn^{3+}$ excitations Eq.(5) at different lattice sites and address the coupling of different AFM–coupled chains and planes (Fig. 1(a)) via quantum spin canting. The latter occurs simultaneously with electron delocalization along the FM chains. We recall that, for classical spins and $J_H \rightarrow \infty$, different chains are uncoupled in the absence of spin canting, leading to 1D electron confinement [11, 25].

We express the quasi–particle excitations $\hat{e}_{nk}$ with momentum k in the form

$$\hat{e}_{nk} = \sum_{i\alpha\sigma} u^n_{k\sigma}(i\alpha) \frac{\hat{e}_{k\sigma}(i\alpha)}{\sqrt{n_{\alpha\sigma}(i)}}, \tag{25}$$

where we introduced the normalization constant

$$n_{\alpha\sigma}(i) = \langle [\hat{e}^\dagger_{k\sigma}(i\alpha), \hat{e}_{k\sigma}(i\alpha)]_+ \rangle = \langle [\hat{e}^\dagger_{\alpha\sigma}(i), \hat{e}_{\alpha\sigma}(i)]_+ \rangle \tag{26}$$

determined by Eq.(23), with average value taken in the reference state. In the CE–AFM background, all spins point parallel to the local z–axes (spin populations M=S+1/2 and m=S only). In the calculations of Fig. 5, these local axes point either parallel or anti–parallel to the laboratory z–axis. Our CE/CO/OO x=1/2 periodic reference state is characterized by a three–dimensional unit cell of 16 sites in two adjacent planes, with two antiferromagnetically–ordered zig–zag FM chains per plane, with four sites per chain, alternating Mn^{3+} and Mn^{4+} atoms, and neigboring planes with opposite spins but identical charge/orbital configurations [11]. For such configuration we obtain from Eq.(23) after using the Glebsch–Gordan coefficients

$$n_{\alpha\uparrow}(i) = \rho^\alpha_i(S+\frac{1}{2}) + \rho_i(S)\ ,\ n_{\alpha\downarrow}(i) = \frac{\rho_i(S)}{\sqrt{2S+1}}. \tag{27}$$

σ=$\uparrow$ corresponds to quasi–electron spin parallel to the reference state local spin, which is always the case in the classical spin limit. $n_{\alpha\uparrow}(i)$ is a phase space filling contribution that prohibits double occupancy, similar to the Gutzwiller wavefunction approximation and slave boson calculations [25]. $n_{\alpha\uparrow}(i)$=1 similar to Ref. [11] if we neglect double–occupancy. More importantly, here σ=$\downarrow$ is also allowed and describes the possibility that the quasi–electron spin may be pointing anti–parallel to the ground state spin, as in the quantum states Eq.(1).

The laser field excites e–h quasi–particles on top of the equilibrium reference state as described in the previous section. We thus seek here e–h eigenmodes of the adiabatic Hamiltonian:

$$i\partial_t \langle \hat{e}^\dagger_{nk} \hat{e}_{mk} \rangle = (\omega_{mk} - \omega_{nk}) \langle \hat{e}^\dagger_{nk} \hat{e}_{mk} \rangle, \tag{28}$$

where the transformed density matrix $\langle \hat{e}^\dagger_{nk} \hat{e}_{mk} \rangle$ is defined by using Eqs.(25) and (6). The time evolution Eq.(20) implies quasi–particle normal modes defined by the following eigenvalue equation:

$$\omega_{km} u^m_{k\sigma}(j\beta) = \varepsilon_{\beta\sigma}(j)\, u^m_{k\sigma}(j\beta) - \sum_{l\alpha} t^k_{\alpha\beta}(l-j) \sqrt{n_{\beta\sigma}(j)}\, \sqrt{n_{\alpha\sigma}(l)}\, \cos\left(\frac{\theta_l - \theta_j}{2}\right) u^m_{k\sigma}(l\alpha)$$
$$+\sigma \sum_{l\alpha} t^k_{\alpha\beta}(l-j) \sqrt{n_{\beta\sigma}(j)}\, \sqrt{n_{\alpha-\sigma}(l)}\, \sin\left(\frac{\theta_l - \theta_j}{2}\right) u^m_{k-\sigma}(l\alpha), \tag{29}$$

where m labels the different quasi–particle branches. σ=+1(-1) means quasi–particle spin parallel (anti–

parallel) to the reference state local spin. In the classical spin limit, $n_{\alpha\downarrow}(i)$=0 and only the first term on the rhs of the above equation survives, which describes energy bands due to coherent hopping amplitude $\propto t^{k}_{\alpha\beta}(l-j)\cos\left(\frac{\theta_l-\theta_j}{2}\right)$ [11, 12, 20]. As in the slave boson [25] and Gutzwiller wavefunction infinite dimensional approximations, the local factors $\sqrt{n_{\alpha\sigma}(l)}$, where here σ=↑,↓, modify these electron hopping amplitudes due to both Hubbard–U and magnetic exchange strong local interactions. Quantum spins introduce an additional coupling between $u_{k\uparrow}$ and $u_{k\downarrow}$, which breaks degeneracies and enhances electron delocalization. As discussed in the main text, these local quantum–spin–canting strong correlations significanly affect the insulator energy gap and energy band dispersions, favoring metallic behavior and FM correlations that strongly depend on E_{JT}.